Review of Scientific Instruments

Femtosecond time-resolved photoemission electron microscopy operated at sample illumination from the rear side

Cite as: Rev. Sci. Instrum. **90**, 053704 (2019); https://doi.org/10.1063/1.5088031
Submitted: 07 January 2019 . Accepted: 20 April 2019 . Published Online: 16 May 2019

Alwin Klick, Malte Großmann, Maria Beewen, Paul Bittorf, Jacek Fiutowski, Till Leißner, Horst-Günter Rubahn, Carsten Reinhardt, Hans-Joachim Elmers, and Michael Bauer

Review of Scientific Instruments ARTICLE scitation.org/journal/rsi

Femtosecond time-resolved photoemission electron microscopy operated at sample illumination from the rear side

Cite as: Rev. Sci. Instrum. 90, 053704 (2019); doi: 10.1063/1.5088031
Submitted: 7 January 2019 • Accepted: 20 April 2019 •
Published Online: 16 May 2019

Alwin Klick,[1,a)] Malte Großmann,[1] Maria Beewen,[1] Paul Bittorf,[1] Jacek Fiutowski,[2] Till Leißner,[2] Horst-Günter Rubahn,[2] Carsten Reinhardt,[3,4] Hans-Joachim Elmers,[5] and Michael Bauer[1]

AFFILIATIONS

[1]Institute of Experimental and Applied Physics, University of Kiel, Leibnizstr. 19, D-24118 Kiel, Germany
[2]NanoSYD, Mads Clausen Institute, University of Southern Denmark, Alsion 2, DK-6400 Sønderborg, Denmark
[3]Laser Zentrum Hannover e.V., Hollerithallee 8, D-30419 Hannover, Germany
[4]Fakultät 4, Hochschule Bremen, Neustadtswall 30, D-28199 Bremen, Germany
[5]Institute of Physics, Johannes Gutenberg University Mainz, Staudingerweg 7, D-55099 Mainz, Germany

[a)]klick@physik.uni-kiel.de

ABSTRACT

We present an advanced experimental setup for time-resolved photoemission electron microscopy (PEEM) with sub-20 fs resolution, which allows for normal incidence and highly local sample excitation with ultrashort laser pulses. The scheme makes use of a sample rear side illumination geometry that enables us to confine the sample illumination spot to a diameter as small as 6 μm. We demonstrate an operation mode in which the spatiotemporal dynamics following a highly local excitation of the sample is globally probed with a laser pulse illuminating the sample from the front side. Furthermore, we show that the scheme can also be operated in a time-resolved normal incidence two-photon PEEM mode with interferometric resolution, a technique providing a direct and intuitive real-time view onto the propagation of surface plasmon polaritons.

I. INTRODUCTION

Femtosecond time-resolved two-photon photoemission electron microscopy (tr2PPEEM) was first demonstrated in 2002.[1] Since then, it has widely been used to track collective electronic excitations and electromagnetic modes in space and time including surface plasmon polaritons (SPPs),[2–5] optical waveguide modes,[6,7] and localized surface plasmons.[8–10] The technique attracted additional interest in the study of carrier transport and recombination in semiconductors.[11,12] Important technological advancements of the technique include the addition of interferometric time resolution,[8] the implementation of energy resolving detection schemes,[13] and the operation at laser illumination in normal incidence as opposed to the standard oblique incidence geometry.[4]

In normal incidence 2PPEEM (NI2PPEEM), the symmetry of the studied problem is not affected by the direction of incidence of the excitation laser. This can be advantageous if one is, for instance, interested in changes in the sample response to the laser polarization.[14,15] Furthermore, when studying propagating electromagnetic modes, the NI2PPEEM signal can provide mode spectral information in a very direct and intuitive manner.[4] Two different excitation schemes of NI2PPEEM are described in the literature: In a front illumination mode, the photoelectrons collected by the PEEM instrument are emitted from the sample surface that is illuminated with the excitation laser.[4] Next to static experiments, this operation mode was in the past particularly successful in interferometric time-resolved studies on the propagation and manipulation of SPP fields.[15,16] In an alternative scheme, the sample is illuminated from the rear side while the PEEM instrument collects photoemitted electrons from the opposite side.[14] Such a configuration relies on the thickness of the investigated sample being of the order of the penetration depth of the excitation laser light, i.e., ultrathin films deposited on transparent substrates have to be used. However, the geometric constraints of this approach are much more relaxed than

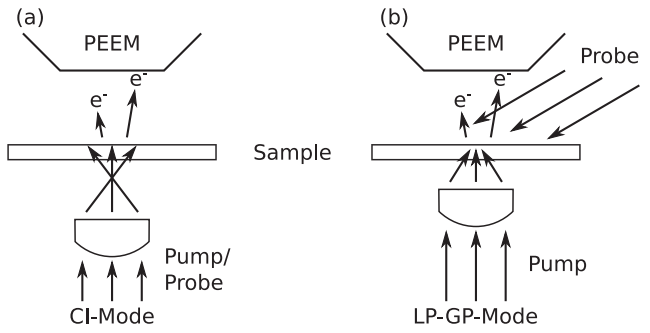

FIG. 1. Schematic illustration of the two PEEM operation modes presented in this work. (a) CI mode: Both laser pulses illuminate the sample in normal incidence from the rear side. To enlarge the illuminated area, the sample surface is positioned at some distance in front of the focal plane of the focusing lens. (b) LP-GP mode: A pump laser pulse is focused in normal incidence from the rear side of the sample. The sample response to the localized excitation is probed by a laser pulse hitting the sample under oblique incidence from the front side.

in the front illumination mode so that highly local excitation conditions using short focal length lenses can be realized at reasonable costs.

The scope of this work is to provide a detailed description and characterization of a novel setup for time-resolved NI2PPEEM that was successfully applied in a recent study on the near-field enhanced photoemission from cross antennas.[14] The experiment is operated in the rear side illumination mode and allows therefore for highly local excitation conditions with the excitation spot size restricted to a diameter of <6 μm. At the same time, pulse broadening effects particularly due to the lens used to focus the excitation laser are kept at a minimum, allowing for excitation of the sample with sub-20 fs laser pulses (FWHM). Two different operation modes are presented (see Fig. 1). In a collinear illumination (CI) mode, pump and probe pulses both hit the sample at normal incidence from the rear side [Fig. 1(a)]. In a local pump/global probe (LP-GP) mode, a large area response of a sample to a highly local laser excitation from the rear side is probed by a time-delayed and weakly focused laser pulse illuminating the sample from the front side [Fig. 1(b)]. The capabilities of the different operation modes are illustrated by examples in which the propagation of SPPs at a gold-vacuum interface is monitored in real time.

II. EXPERIMENTAL DETAILS

A. System configuration

The setup demonstrated in the present work is based on an oblique incidence tr2PPEEM system introduced in detail in Ref. 17. We use a commercial photoemission electron microscope (IS PEEM, *Focus GmbH*) mounted inside an ultrahigh vacuum (UHV) μ-metal chamber (base pressure: 1×10^{-10} mbar). Experiments are performed with a sub-15 fs Ti:sapphire oscillator (Griffin, *KMLabs*) operated at a center wavelength $\lambda \approx 775$ nm ($h\nu = 1.6$ eV). Measurement of the laser beam profile in mode-locked operation and in front of the entrance window of the UHV chamber yields a beam size (FWHM) of 1.4 mm in the vertical direction and 1.8 mm in the horizontal direction.

In the CI mode, the laser pulses are equally split into two pulses using an actively stabilized Mach-Zehnder interferometer,[18] allowing for adjusting the time delay τ between the two pulses with an accuracy of <30 as.[3] The two pulses are collinearly focused onto the sample from the rear side using a focusing device introduced in detail below. When operated in the LP-GP mode, a beam splitter separates the pulses into a pump part that is focused onto the sample from the rear side. The other (probe) part hits the sample under oblique incidence from the front side after passing through an adjustable delay stage. In both operation modes, group velocity dispersion (GVD) of the laser pulses are compensated by a Fork prism compressor. This includes GVD picked up during propagation from the optical components of the setup, from the UHV entrance window and during propagation through air.[19]

B. Samples

Three different types of samples were used in the experiments described below. For the characterization of laser spot size and pulse width at the sample position, 40 nm thick polycrystalline gold films were evaporated onto a 1.1 mm fused silica (FS) substrate covered with a 100 nm thick indium tin oxide (ITO) layer (sample A). For the experiments performed in the CI mode, quadratic gold platforms ($100 \times 100\ \mu m^2$, 50 nm thickness) were fabricated onto the ITO/FS substrate by standard UV photolithography (sample B). Experiments in the LP-GP mode were performed with 50 nm thick polycrystalline gold films evaporated onto dielectric ridges made from Ormosil[20] (sample C). The ridges were lithographically structured using mask projection microscope photolithography, providing sub-200 nm resolution.[21–24] In all three samples, an ultrathin chromium adhesion layer between the gold film and substrate was used.

Prior to the 2PPEEM experiments, a sub-monolayer of cesium was deposited *in situ* onto the sample surface from a well-degassed getter source (*SAES Getters*). This procedure was used to lower the work function of the gold film below a value of 3.2 eV so that two-photon photoemission (2PPE) with the 775 nm laser source becomes possible. In past studies, we have shown that the deposition of small amounts of cesium onto a gold sample does not affect the propagation properties of SPPs within the resolution of the PEEM instrument.[25]

C. Focusing device

Illumination of the sample from the rear side with a focused, normal incident laser beam becomes possible with the installation of a home-built focusing device into the UHV chamber, which has also been used in the above mentioned study on near-field photoemission.[14] We would like to note that in comparison with the setup used in the latter study, the performance of the focusing device has been further improved. A careful selection of the focusing lens parameter as described in detail below allowed to considerably reduce the achievable focal spot size by more than a factor of 10. At the same time, the ultimate temporal resolution of the experiment could be improved by more than factor of 5 and was pushed into the sub-20 fs regime. Additionally, an optical setup capable of interferometric resolution was successfully implemented into the experimental setup. A schematic of the device is shown in Fig. 2. It is mounted to the vacuum flange opposite to the entrance lens of the PEEM. The laser beam enters the UHV-system through a fused silica entrance

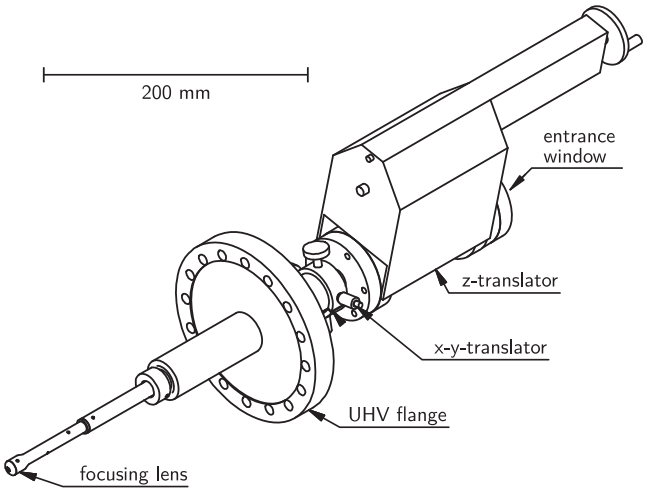

FIG. 2. Schematic of the focusing device. The laser beam enters the UHV through the entrance window, passes an evacuated pipe, and is focused onto the sample (not shown) from the rear by the focusing lens mounted to the end of the pipe. Translator stages allow positioning the lens in the x-, y-, and z-direction with an accuracy of ≈10 μm. The pipe is fully retractable to not impede sample stage movement or when the focusing device is not needed.

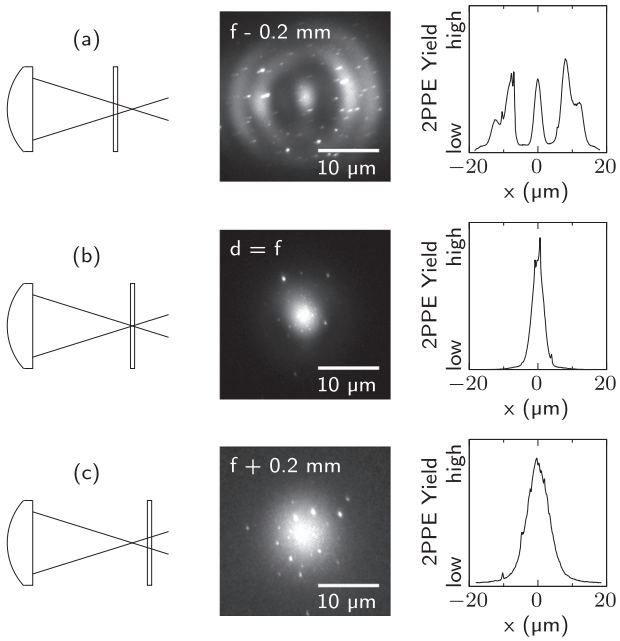

FIG. 3. Characterization of the excitation spot profile at the sample surface: 2PPEEM images and 2PPE intensity profiles of a plane gold surface (sample A) for different positions of the sample surface with respect to the position f of the focal plane. The excitation geometry is schematically illustrated in the left column. (a) Sample positioned at $f - 0.2$ mm: The 2PPE intensity pattern is modulated by distinct interference rings. (b) Sample positioned in the focal plane: The minimum 2PPE spot diameter of 3.85 μm is observed corresponding to a laser spot diameter of 5.5 μm (FWHM). (c) Sample positioned at f + 0.2 mm: The 2PPE spot diameter becomes enlarged without disturbing interference rings. The bright dots in the 2PPEEM images are due to defects of the gold film.

window and passes an evacuated pipe. A planoconvex lens mounted to the end of the pipe is used to focus the beam from the rear side onto the sample. A three-axis translation stage allows for an accurate positioning of the incident beam onto the sample with a reproducibility of 0.01 mm. An overall stroke of 10 cm along the z-direction additionally allows us to completely retract the focusing lens out of the sample area if required.

The focusing device should finally deliver a laser spot diameter of a few micrometers at the sample position while keeping the laser pulse width in the sub-20 fs regime. We chose fused silica as the lens material as in the near infrared spectral regime, chromatic dispersion and GVD of this material are both comparatively small. A small chromatic dispersion minimizes chromatic aberration effects, which at broadband illumination can considerably broaden the focal diameter. Due to lack of UHV-compatibility, achromatic lenses cannot be used in the setup. A small GVD reduces temporal broadening effects during passage of the ultrashort laser pulses through the lens. In this work, a lens radius of curvature $R = 7.5$ mm was chosen, yielding for 775 nm light a focal length $f = 16.54$ mm and for a beam diameter $d = 1.6$ mm (FWHM) a focal diameter of 3.61 μm. The latter value was calculated under the assumption of an incident monochromatic Gaussian beam and represents therefore a lower limit of the excitation spot diameter that we expect in the experiment for the given beam cross section.

Figures 3(a)–3(c) compare 2PPEEM images from sample A at laser illumination from the sample rear side and for different distances between the sample surface and focal plane of the fused silica lens. The images were recorded from a plane area of the gold film using broadband laser pulses (775 nm central wavelength), supporting a transform-limited pulse width of ≈12 fs. As we increase the lens-sample distance, size and shape of the photoemission spot profile undergo clear changes. We measure a minimum spot diameter of 3.85 μm (FWHM) in the 2PPEEM signal when the sample surface is positioned in the focal plane [see the 2PPE intensity profile in Fig. 3(b)]. Under consideration of the second order nonlinearity of the 2PPE process, this yields an actual laser spot diameter at the sample surface of 5.5 μm (FWHM). This value exceeds the estimated minimum diameter by a factor of ≈1.5 most likely due to chromatic aberration at broadband illumination and deviations from a Gaussian beam profile. The ringlike pattern observed for the case when the sample is positioned between the lens and focal plane [Fig. 3(a)] arises from combined refraction and interference effects at the glass substrate of the sample. The pattern is very useful for the adjustment of the laser beam to normal incidence, as already small deviations from normal incidence conditions distort its radial symmetry. Experiments performed in the CI mode typically rely on the illumination of extended sample areas instead of highly local excitation conditions. For this type of experiments, the focal plane is positioned between the lens and sample so that at the sample surface an enlarged illumination spot without interference rings is formed [Fig. 3(c)].

GVD, which is governed by the second derivative of the refractive index, $d^2n/d\lambda^2$, is the dominant contribution to the temporal broadening of ultrashort pulses when propagating through plane optics. The situation gets more complex in the case of lenses.

At increasing distance from the optical axis, the path length through the material will decrease so that different parts of the beam will accumulate different amounts of GVD. The variation in the propagation length through the material will furthermore result in a variation in the delay between the group and phase front, resulting in an additional broadening of the pulse at the focal point. This effect is also referred to as propagation time difference (PTD) and is proportional to $dn/d\lambda$.[26] The latter two effects cannot be compensated by conventional pulse compression schemes, such as Fork prism compressors or grating compressors, and must, therefore, be tolerated in the final configuration of the setup. Figure 4(a) shows how the GVD that is accumulated by the laser beam during propagation through the fused silica lens changes as a function of distance r from the optical axis. The data were calculated for a wavelength of 800 nm. At $r = d/2 = 0.8$ mm, we expect the GVD of the passed laser beam being 1.3 fs^2 smaller than at the lens center [see the black line and arrow in Fig. 4(a)]. For a transform-limited incident 15 fs-laser pulse, this value results in a difference in the pulse width of only ≈0.005 fs, indicating the minor relevance of this effect for the time-resolution of the experiment.

Even though small, calculations show that PTD effects are of more significance. Figure 4(b) displays the amount of delay T_0 between the group and phase front accumulated during propagation through the lens as a function of distance from the optical axis calculated for a wavelength of 800 nm. For instance, at $r = d/2 = 0.8$ mm, T_0 is reduced by ≈2 fs in comparison with the value of T_0 at the optical axis [see the black line and arrow in Fig. 4(b)]. Figure 4(c) shows how the temporal profile of a laser pulse is affected in the presence of PTD. For the calculations, we considered a transform-limited 15 fs-laser pulse with a Gaussian intensity profile [beam diameter of 1.6 mm (FWHM)]. The results show that the exit pulse is broadened due to PTD effects by ≈0.5 fs in comparison with the incidence pulse. Additionally, the pulse profile becomes slightly asymmetric as a tail forms at the pulse front end. Notably, the distortion of the pulse profile quickly grows as the beam diameter increases. For a beam diameter of 3.2 mm (FWHM), we expect that the exit pulse is broadened by 2.9 fs with the front end tail being much more pronounced [see the blue line in Fig. 4(c)]. However, an increase in the beam diameter can at the same time reduce the spot diameter at the sample position. The beam diameter of the incident laser pulse is therefore a critical parameter in the experiment and has to be adjusted for an optimum trade-off between temporal resolution and lateral extension of the sample excitation spot.

Characterization of the temporal pulse profile was performed by second order interferometric autocorrelation (IAC) measurements. Second harmonic generation (SHG) IAC traces were measured using a β-Barium Borate (BBO) crystal before the pulse enters the UHV chamber. 2PPE IAC traces derived from interferometric tr2PPEEM data from sample A were additionally used to characterize the temporal pulse profile at the sample position. 2PPE IAC traces were recorded in the CI mode, i.e., upon illumination of sample A from the rear side. For reference, we additionally recorded 2PPE IAC traces at collinear illumination of sample A from the front side in the conventional oblique incidence geometry. In all measurements, the Fork prism compressor was adjusted to minimize GVD effects.

Figures 5(a)–5(c) compare experimental interferometric SHG and 2PPE IAC traces. The width of the SHG IAC signal envelope [Fig. 5(a)] yields a temporal width of ≈13.5 ± 0.5 fs (FWHM)[27] for the laser pulses entering the UHV chamber, a value close to the transform limit of 11.5 fs determined from the laser spectrum. Analysis of the 2PPE traces yield values of 14.9 ± 1 fs and 16.7 ± 1 fs for sample front illumination [Fig. 5(b)] and CI illumination [Fig. 5(c)], respectively. These values are slightly larger than what is observed in the SHG IAC measurements. In both cases, we particularly note

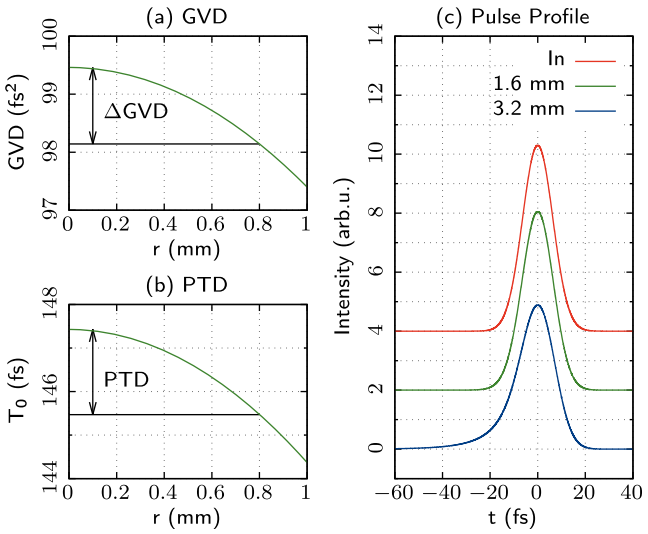

FIG. 4. Pulse broadening effects due to the focusing lens. (a) GVD accumulated at 800 nm wavelength during passage through the focusing lens as a function of distance r from the optical axis. (b) Time delay between the group and phase front after passage of 800 nm-laser light as a function of distance r from the optical axis. (c) Changes in the pulse profile of an initially transform-limited laser pulse (15 fs pulse width, 800 nm center wavelength, and 1.6 mm beam diameter) due to PTD at passage through the lens. Solid red line: incident pulse profile; solid green line: exit pulse profile. The blue line shows the exit pulse profile for a beam diameter of 3.2 mm.

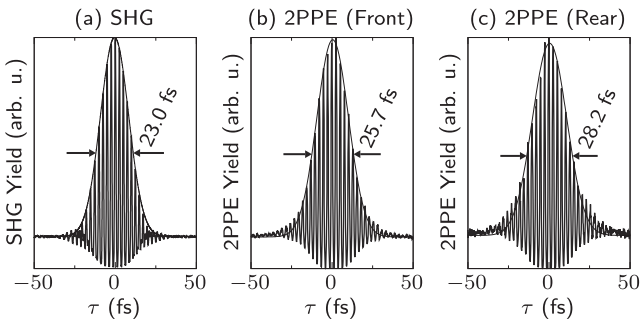

FIG. 5. Experimental second order IACs. (a) SHG IAC measured at the interferometer output. 5 mm of fused silica was inserted into the beam path to account for material dispersion due to different components in the 2PPEEM setup. (b) 2PPE IAC traces derived from interferometric tr2PPEEM data from sample A recorded at front illumination in the conventional oblique incidence mode. (c) 2PPE IAC traces derived from interferometric tr2PPEEM data from sample A recorded in the CI mode. For all three measurements, the Fork prism compressor was adjusted to minimize GVD effects. Gaussian fits to the IAC envelopes are added to the graphs. Numbers indicate the width Δt_{IAC} (FWHM) of the Gaussians.

some broadening at the tail of the traces which we assign to the finite lifetime of the excited intermediate quasiparticle states probed in the 2PPE process.[28] The difference between the two 2PPE traces may hint to PTD effects in the presence of the focusing lens in the CI mode. However, it should also be noted that some left over GVD is visible in the data recorded in the CI mode which could not completely be compensated by the Fork prism compressor. Nevertheless, the data show that also in the CI mode the laser pulse width can be kept well in the sub-20 fs range, proving the capability of this approach to perform interferometric tr2PPEEM experiments at high temporal resolution.

III. OPERATION MODES

A. CI mode

In the CI mode, two collinear and time-delayed equal pulses illuminate the rear side of the sample at normal incidence. The focusing lens is positioned at a distance of $f + 0.6$ mm from the sample surface so that the focal plane is located between the lens and surface [see Fig. 3(c)]. This excitation geometry results in a homogeneous and extended illumination spot with a diameter of ≈80 μm. For the test experiments, we excited SPP wave packets at sample B by illuminating an edge of a gold platform with the polarization of the two excitation pulses oriented perpendicular to the edge. The time delay τ between the two pulses was varied from $\tau = +25$ fs to $\tau = +60$ fs in steps of 0.2 fs. For each time delay, a 2PPEEM image of the illuminated sample area was captured.

Figures 6(a) and 6(b) show 2PPEEM images recorded at $\tau = +30$ fs and $\tau = +55$ fs. The periodic intensity pattern emerging from the illuminated (coupling) edge of the gold platform [marked CE in Figs. 6(a) and 6(b)] is the characteristic photoemission signature of the excited SPP wave packet.[2] In PEEM experiments performed under normal incidence, the wavelength of the probed SPP can directly be read out from the periodicity of this pattern.[4] In a two-pulse correlation experiment, an SPP pattern is formed from two different contributions:[2] In the vicinity of the coupling edge, one observes a static signal which does not evolve as τ is varied and which results from the superposition of the SPP wave packet with the laser pulse it is excited from. The second component arises from the superposition of the same SPP wave packet with the second laser pulse. This part of the pattern propagates along the surface as τ is varied [see differences between Figs. 6(a) and 6(b) marked by the arrow] and contains the relevant time-domain information on phase and group propagation of the SPP.

Figure 6(c) shows a delay-distance diagram which plots 2PPE intensity profiles as a function of τ and distance x from the coupling edge. The intensity profiles were derived from the complete interferometric CI scan and were generated by integration along the vertical axis of the 2PPEEM images. In this representation of the data, the propagation of an SPP wave packet results in a sloped interference pattern with the slope of the interference maxima (and minima) determined by the SPP phase velocity v_{ph}.[3] Notably, the data show two patterns which clearly differ in their slope, indicating that two different SPP modes are excited at the coupling edge. We assign the dominating interference pattern, which in the graph extends to the maximum propagation distance probed in the experiment, to an SPP which is excited at the gold-vacuum interface [see the blue line in Fig. 6(c)]. The quantitative analysis of the data yields for this mode

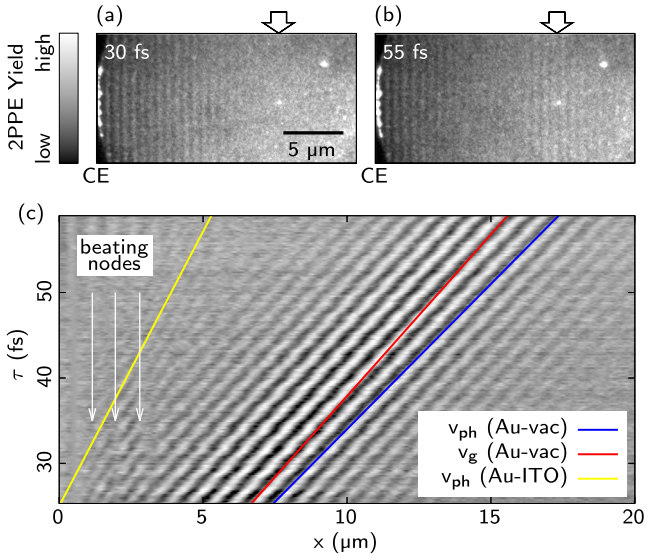

FIG. 6. tr2PPEEM data of sample B recorded in the CI mode. [(a) and (b)] 2PPEEM images at $\tau = 30$ fs and $\tau = 55$ fs. The differences in the periodic intensity pattern particularly in the part of the images marked by the arrow result from the propagation of an SPP wave packet excited at the coupling edge (CE). (c) Delay-distance diagram compiled from a complete interferometric tr2PPEEM scan. The graph shows 2PPE intensity profiles of individual 2PPEEM images after background subtraction and normalization to maximum intensity as a function of τ and distance x from the coupling edge. The blue (yellow) line indicates the slope of the interference pattern determined by the phase velocity of an SPP propagating along the gold-vacuum (gold-ITO) interface. The red line indicates the slope of the pattern envelope maximum determined by the group velocity of the gold-vacuum SPP. Beating nodes arising from the superposition of gold-vacuum and gold-ITO SPPs are marked by white arrows.

an effective index $n_{eff} = 1.02$ and a phase velocity $v_{ph} = 0.98c$, with c being the vacuum speed of light. The latter value conforms with the calculated value for a gold-vacuum SPP under consideration of reference permittivity data of gold.[29] The slope of the line following the envelope maximum of the pattern [see the red line in Fig. 6(c)] is determined by the SPP group velocity v_g.[3] Here, the quantitative analysis yields a value of $v_g = 0.93c$ once again in good agreement with the expectation for a gold-vacuum SPP.

The second pattern is visible for distances $x < 5$ μm. The slope of the interference maxima of this pattern is significantly steeper than what is observed for the gold-vacuum SPP [see the yellow line in Fig. 6(c)]. The quantitative analysis of this pattern yields an effective index of $n_{eff} = 1.93$ corresponding to $v_{ph} = 0.52c$. A comparison with calculations shows that the second pattern arises from the excitation of an SPP at the buried interface between the gold layer and ITO film. For the calculations, we used permittivity data of ITO from Ref. 30. The observation of an interface SPP hidden underneath a gold layer using PEEM was so far only reported in experiments using high quality (single crystalline) gold platelets of a thickness of 20 nm.[31] The high sensitivity of the present experiment (which was conducted with a 50 nm thick polycrystalline gold film) results from the rear illumination geometry, which strongly favors SPP excitation at the gold-ITO interface in comparison with excitation at the gold-vacuum surface owing to the limited penetration depth of

≈13 nm of 800 nm light into the gold film.[29] Notably, we also observe an interference between the two SPPs. The resulting beating nodes are indicated by the white arrows in Fig. 6(c). The observed beating period of 0.9 ± 0.1 μm agrees very well with a calculated value of 0.85 μm considering the evaluated effective indices of the two involved modes.

B. LP-GP mode

In the LP-GP mode, a pump laser pulse illuminates the sample in normal incidence from the rear. The sample surface is positioned in the focal plane guaranteeing a highly local excitation confined to an area of ≈16 μm^2. The response of the sample to the excitation is probed by a second laser pulse illuminating the sample at an angle of incidence $\Theta = 65°$ with respect to the surface normal from the front side. A concave mirror (500 mm focal length) is used to focus the probe beam restricting the illuminated area to a size of ≈5400 μm^2. For the measurement shown here, a dielectric ridge of sample C was moved into the pump excitation area with the pump pulse polarized perpendicular to the ridge in order to excite SPP wave packets. 2PPEEM images of the sample recorded at simultaneous illumination with the pump and probe beam at different time delays τ are shown in Fig. 7(a), with the p-polarized probe beam incident from the left. The time delays between the pump and probe beam were set to $\tau = -33.3$ fs, 20.0 fs, and 206.7 fs, respectively. In the images, photoemission signals from different processes are visible. The excitation by the pump pulse results in a bright photoemission spot located on top and in the close vicinity of the ridge. The faint short-period intensity patterns within this spot on both sides of the ridge are the static signals of SPPs which are excited and probed by the pump pulse at the same time. The long-period intensity pattern to the right of the ridge is the corresponding static signal of an SPP that is excited and probed by the probe pulse.[2] Close to time-zero, i.e., at $\tau = -33.3$ fs (20.0 fs), additional short-period interference fringes appear on the right (left) hand side of the excitation ridge. These fringes result from the interference between the normal incidence pump and oblique incidence probe pulse, marking for a given value of τ the area of spatiotemporal overlap between the two pulses, as will be discussed below. At sufficiently large delays, i.e., at $\tau = 206.7$ fs, the area of spatiotemporal overlap has left the field of view and no cross correlation signal between pump and probe pulses is visible any more.

For time-resolved LP-GP experiments, τ was varied between −100 fs and 200 fs with respect to time zero in steps of 6.67 fs. Here, a negative time delay denotes the case in which the probe pulse arrives at the pump excitation area before the pump pulse. The result of a complete time-resolved LP-GP scan is summarized in the time-distance diagram shown in Fig. 7(b). Similar to Fig. 6(c), the diagram plots 2PPE intensity profiles as a function of τ and distance x from the excitation ridge for a complete pump-probe scan. The intensity profiles were once again generated by integration along the vertical axis of the 2PPEEM images. For each x-value, the data were normalized along the time-delay axis. This procedure effectively suppresses the strong and localized photoemission signal from the focused pump pulse as well as the static interference patterns from the pump and probe pulses.

Over the entire x-range, the data plotted in Fig. 7(b) are dominated by a linear signal trace extending from $\tau = 100$ fs to $\tau = -100$ fs.

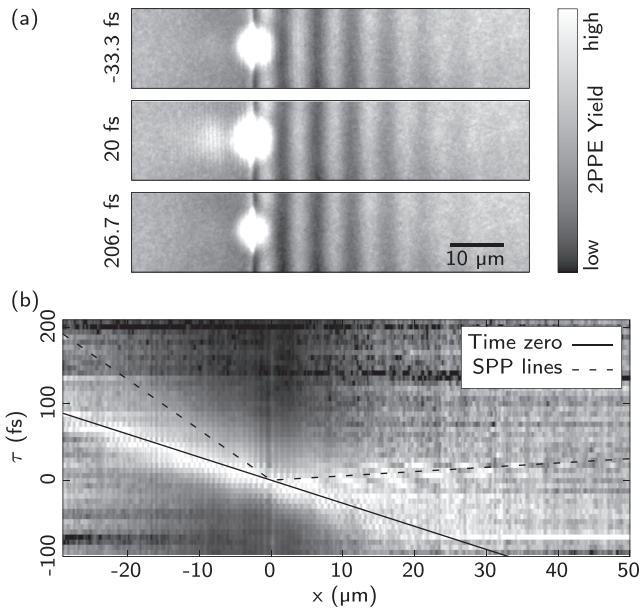

FIG. 7. tr2PPEEM data of sample C recorded in the LP-GP mode. (a) 2PPEEM images recorded with a focused pump beam illuminating a dielectric ridge of the sample from the rear side and an oblique incident probe beam illuminating the sample from the front side at different time delays τ. The short-period fringe pattern visible to the right (left) of the bright excitation spot at $\tau = -33.3$ fs ($\tau = 20$ fs) results from a cross correlation signal between pump and probe pulses. (b) Delay-distance diagram compiled from a complete tr2PPEEM scan. The graph shows 2PPE intensity profiles of individual 2PPEEM images after background subtraction and normalization to maximum intensity as a function of τ and distance x from the excitation ridge. For each time delay, the 2PPEEM signal was integrated vertically. The black solid line marks the signal arising from the cross correlation between the pump-laser signal diffracted into the sample surface plane and the probe laser pulse. The line marks at the same time the actual time-zero of the experiment. The two dashed lines mark the pump-probe cross correlation signal resulting from propagating SPP wave packets excited by the focused pump pulse at the sample ridge and propagating in the opposite direction. The slopes of the dashed lines are determined by the SPP group velocity.

The slope of the signal, $\frac{\Delta\tau}{\Delta x}$, can be related to the probe beam surface projection of the vacuum speed of light, c_p, and is given by $\frac{\Delta\tau}{\Delta x} = -\frac{1}{c_p} = -\frac{\sin\Theta}{c} = -3.02\,\text{fs}\,\mu\text{m}^{-1}$ [see the black solid line in Fig. 7(b)]. We obviously detect here the cross correlation of the pump laser signal diffracted into the sample surface plane and the probe laser pulse. The signal trace marks the actual time zero of the experiment, which varies along the x-direction due to the oblique incidence of the probe beam and the resulting spread in the probe pulse arrival time along the sample surface. We conclude that any dynamics associated with the localized excitation of SPPs by the pump pulse can only show up in the area of the time-distance diagram above the time zero line, where at the probed position the probe pulse follows the pump pulse. In this area, we identify two different signatures arising from SPP excitation, emerging in the opposite direction from the pump excitation area at $x = 0$ and marked by black dashed lines in Fig. 7(b). We monitor here the group propagation of SPP wave packets that are excited by the focused pump beam at the ridge and that propagate into the positive and negative x-direction. The comparison of the

slope of the respective signal traces with calculations under consideration of the SPP group velocity $v_g = 0.93c$ at a gold-vacuum interface for excitation with 800 nm light[3] confirms this interpretation. For the SPP wave packet copropagating with the probe pulse, i.e., propagating in the positive x-direction, the slope of the signal trace in a time-distance diagram is given by $\frac{\Delta\tau}{\Delta x} = \frac{1}{v_g} - \frac{1}{c_p}$,[3] yielding a value of $\frac{\Delta\tau}{\Delta x} = 0.56$ fs μm^{-1}. For a counterpropagating SPP wave packet, i.e., a wave packet propagating in the negative x-direction, the slope of the signal trace in a time-distance diagram is given by $\frac{\Delta\tau}{\Delta x} = \frac{1}{v_g} + \frac{1}{c_p}$,[3] yielding a value of $\frac{\Delta\tau}{\Delta x} = 6.61$ fs μm^{-1}. For the direct comparison with the experimental data, the slopes of the black dashed lines in Fig. 7(b) were set accordingly.

IV. CONCLUSION

We presented an advanced experimental setup for time-resolved PEEM in which a thin film sample deposited onto a transparent substrate is excited in normal incidence with an ultrashort laser pulse from the rear side. Despite the use of a short focal length lens in the experimental setup, we succeeded in keeping pulse broadening effects at a tolerable level while at the same time highly local excitation conditions could be achieved. We successfully demonstrated two modes of operation: Operated in a collinear illumination mode, the setup allows for interferometric normal-incidence 2PPEEM experiments, a scheme which in the study of SPP propagation can be advantageous in comparison with conventional oblique incidence PEEM.[4] In a local pump-global probe mode, the spatiotemporal evolution of a highly local photoexcitation is globally probed by a laser pulse incident onto the sample front side. We particularly expect the latter operation mode to be of interest for studies beyond the investigation of SPP excitations such as the study of carrier transport dynamics in semiconducting materials.

ACKNOWLEDGMENTS

This work was supported by the German Research Foundation (DFG) through Priority Program No. 1391 "Ultrafast Nanooptics" and Projects Nos. RE3012/4-1 and RE3012/2-1.

REFERENCES

[1] O. Schmidt, M. Bauer, C. Wiemann, R. Porath, M. Scharte, O. Andreyev, G. Schönhense, and M. Aeschlimann, Appl. Phys. B **74**, 223 (2002).
[2] A. Kubo, N. Pontius, and H. Petek, Nano Lett. **7**, 470 (2007).
[3] C. Lemke, T. Leißner, S. Jauernik, A. Klick, J. Fiutowski, J. Kjelstrup-Hansen, H.-G. Rubahn, and M. Bauer, Opt. Express **20**, 12877 (2012).
[4] P. Kahl, S. Wall, C. Witt, C. Schneider, D. Bayer, A. Fischer, P. Melchior, M. Horn-von Hoegen, M. Aeschlimann, and F.-J. Meyer zu Heringdorf, Plasmonics **9**, 1401 (2014).
[5] Y. Gong, A. G. Joly, D. Hu, P. Z. El-Khoury, and W. P. Hess, Nano Lett. **15**, 3472 (2015).
[6] J. P. S. Fitzgerald, R. C. Word, S. D. Saliba, and R. Könenkamp, Phys. Rev. B **87**, 205419 (2013).
[7] R. C. Word and R. Könenkamp, Opt. Express **24**, 18727 (2016).
[8] A. Kubo, K. Onda, H. Petek, Z. Sun, Y. S. Jung, and H. K. Kim, Nano Lett. **5**, 1123 (2005).
[9] M. Bauer, C. Wiemann, J. Lange, D. Bayer, M. Rohmer, and M. Aeschlimann, Appl. Phys. A **88**, 473 (2007).
[10] M. Aeschlimann, M. Bauer, D. Bayer, T. Brixner, F. Javier Carcia de Abajo, W. Pfeiffer, M. Rohmer, C. Spindler, and F. Steeb, Nature **446**, 301 (2007).
[11] K. Fukumoto, K. Onda, Y. Yamada, T. Matsuki, T. Mukuta, S.-I. Tanaka, and S.-Y. Koshihara, Rev. Sci. Instrum. **85**, 083705 (2014).
[12] K. Fukumoto, Y. Yamada, K. Onda, and S. Koshihara, Appl. Phys. Lett. **104**, 053117 (2014).
[13] A. Oelsner, M. Rohmer, C. Schneider, D. Bayer, G. Schönhense, and M. Aeschlimann, J. Electron Spectrosc. Relat. Phenom. **178**, 317 (2010).
[14] P. Klaer, G. Razinskas, M. Lehr, X. Wu, B. Hecht, F. Schertz, H. J. Butt, G. Schönhense, and H. J. Elmers, Appl. Phys. B **122**, 136 (2016).
[15] G. Spektor, D. Kilbane, A. K. Mahro, B. Frank, S. Ristok, L. Gal, P. Kahl, D. Podbiel, S. Mathias, H. Giessen, F.-J. Meyer zu Heringdorf, M. Orenstein, and M. Aeschlimann, Science **355**, 1187 (2017).
[16] P. Kahl, D. Podbiel, C. Schneider, A. Mahris, S. Sindermann, C. Witt, D. Kilbane, M. Horn-von Hoegen, M. Aeschlimann, and F. Meyer zu Heringdorf, Plasmonics **13**, 239 (2018).
[17] T. Leißner, K. Thilsing-Hansen, C. Lemke, S. Jauernik, J. Kjelstrup-Hansen, M. Bauer, and H.-G. Rubahn, Plasmonics **7**, 253 (2012).
[18] M. U. Wehner, M. H. Ulm, and M. Wegener, Opt. Lett. **22**, 1455 (1997).
[19] R. L. Fork, O. E. Martinez, and J. P. Gordon, Opt. Lett. **9**, 150 (1984).
[20] A. Ovsianikov, J. Viertl, B. Chichkov, M. Oubaha, B. MacCraith, I. Sakellari, A. Giakoumaki, D. Gray, M. Vamvakaki, M. Farsari, and C. Fotakis, ACS Nano **2**, 2257 (2008).
[21] T. Birr, U. Zywietz, P. Chhantyal, B. N. Chichkov, and C. Reinhardt, Opt. Express **23**, 31755 (2015).
[22] T. Birr, U. Zywietz, T. Fischer, P. Chhantyal, A. B. Evlyukhin, B. N. Chichkov, and C. Reinhardt, Appl. Phys. B **122**, 164 (2016).
[23] J. C. Love, D. B. Wolfe, H. O. Jacobs, and G. M. Whitesides, Langmuir **17**, 6005 (2001).
[24] R. Orghici, K. Bethmann, U. Zywietz, C. Reinhardt, and W. Schade, Opt. Lett. **41**, 3940 (2016).
[25] C. Lemke, T. Leißner, A. Klick, J. Fiutowski, J. W. Radke, M. Thomaschewski, J. Kjelstrup-Hansen, H.-G. Rubahn, and M. Bauer, Appl. Phys. B **116**, 585 (2014).
[26] Z. Bor, Opt. Lett. **14**, 119 (1989).
[27] We assume $\Delta t_{pulse}/\Delta t_{IAC} \approx 1.7$ as expected for a Gaussian pulse close to the transform limit, *Springer Handbook of Lasers and Optics*, 2nd ed., edited by F. Träger (Springer Science & Business Media, 2012).
[28] M. Bauer, A. Marienfeld, and M. Aeschlimann, Prog. Surf. Sci. **90**, 319 (2015).
[29] P. B. Johnson and R. W. Christy, Phys. Rev. B **6**, 4370 (1972).
[30] R. J. Moerland and J. P. Hoogenboom, Optica **3**, 112 (2016).
[31] B. Frank, P. Kahl, D. Podbiel, G. Spektor, M. Orenstein, L. Fu, T. Weiss, M. Horn-von Hoegen, T. J. Davis, F.-J. Meyer zu Heringdorf, and H. Giessen, Sci. Adv. **3**, e1700721 (2017).